# PET imaging of adenosine A2A receptors

Zhou, Xiaoyun

# Chapter 1

# General introduction

## ADENOSINE AND ADENOSINE RECEPTORS IN THE CENTRAL NERVOUS SYSTEM

Our brain is wired with hundred billions of neurons, the highway of information transduction, and 10 to 50 times more glial cells (astrocytes, oligodendrocytes, and microglia are main types of glial cells) supporting and nurturing neurons. Information carried by nerve impulses, flows from one neuron to another by passing neurotransmitters through the synapses between them. Adenosine can act as a neuromodulator or neurotransmitter and is formed by the breakdown of adenosine triphosphate (ATP), the main energy source of the body. Adenosine inhibits neuronal excitation in central nervous system (CNS) in general. Therefore caffeine, which blocks the effects of adenosine, can make you feel excited, energetic, and alert. Adenosine exists both inside and outside of the cell, functioning through binding to four types of adenosine receptors, denoted $A_1$, $A_{2A}$, $A_{2B}$, and $A_3$. Adenosine receptors are localized at the cell membrane, belonging to the family of G-protein coupled receptors. These receptors are stimulated by their ligands (*e.g.,* adenosine) outside the cell, triggering signaling pathways inside the cell via activation of receptor associated G-proteins. The G-protein consists of three units, namely α, β and γ unit. The function of a G-protein coupled receptor depends on the type of α subunit which attaches to the receptor. Adenosine $A_1$ and $A_{2B}$ receptors are coupled with $G_{\alpha i/o}$ and function in an opposite manner to $A_{2A}$ and $A_3$ receptors [1,2], which are coupled with $G_{\alpha s}$, in controlling adenylyl cyclase (AC). Among the four adenosine receptor subtypes, adenosine $A_1$ receptor ($A_1R$) and adenosine $A_{2A}$ receptor ($A_{2A}R$) are studied best, because of their abundant expression in the CNS. $A_1Rs$ are found to be widespread throughout the brain, with the highest levels in hippocampus, cerebellum, and cerebral cortex. $A_{2A}R$ are highly enriched in striatum, and scarcely expressed in other brain regions [2]. $A_{2B}$ and $A_3$ receptors are expressed at low levels in the CNS, with functions largely unknown. $A_1R$ and $A_{2A}R$ act oppositely on neurotransmitter release. $A_1R$ activation suppresses neurotransmission, whereas $A_{2A}R$ activation facilitates neurotransmission. Apart from the important role of $A_{2A}R$ on regulating neurotransmission, $A_{2A}R$ has gained pharmacological interest because of its association with the dopamine $D_2$ receptor ($D_2R$). Furthermore, $A_1R$ and $A_{2A}R$ are not only expressed by neurons, but are also present on glial cells, where they have opposite effects on astrogliosis (astrogliosis is an abnormal increase of the number of astrocytes due to neuronal damage) [3]. Glial $A_{2A}R$ is involved in neuroinflammation [3,4], which is a common factor in many brain disorders, such as autism [5], schizophrenia [6], Alzheimer's disease (AD) [7], Parkinson's disease (PD) [8] and

multiple sclerosis [9].

## ADENOSINE $A_{2A}$ RECEPTORS AS PHARMACOLOGICAL TARGET AND DIAGNOSTIC BIOMARKER IN BRAIN DISORDERS

### Pharmacological importance of adenosine $A_{2A}$ receptors

$A_{2A}$Rs are distributed restrictively in striatum, with the highest density in dorsal striatum, a brain region associated with motor functions, and lower levels in ventral striatum, which is part of the reward system. The major physiological role of $A_{2A}$R is believed to modulate locomotor activities, which makes it an interesting therapeutic target in brain disorders associated with movement deficits [10].

In striatum, a large number of $A_{2A}$Rs form functional heteromers (a heteromer is a complex composed of two or more different proteins) with $D_2$Rs at the postsynaptic region (**Figure 1.1**) [11]. $D_2$R is a subtype of the dopamine receptor, and like $A_{2A}$R, a member of the G-protein coupled receptor family. When a $D_2$R ligand (*e.g.,* dopamine) binds to a $D_2$R, a secondary signaling pathway is triggered, resulting in inhibition of neural firing (neural firing is the neuron reacting on stimulation) by negative modulation of NMDA receptor-mediated $Ca^{2+}$ signaling (**Figure 1.2**) [12]. $A_{2A}$R, on the contrary, facilitates neuronal excitation. Ligand binding to $A_{2A}$R or $D_2$R in the heterodimer complex induces a conformational

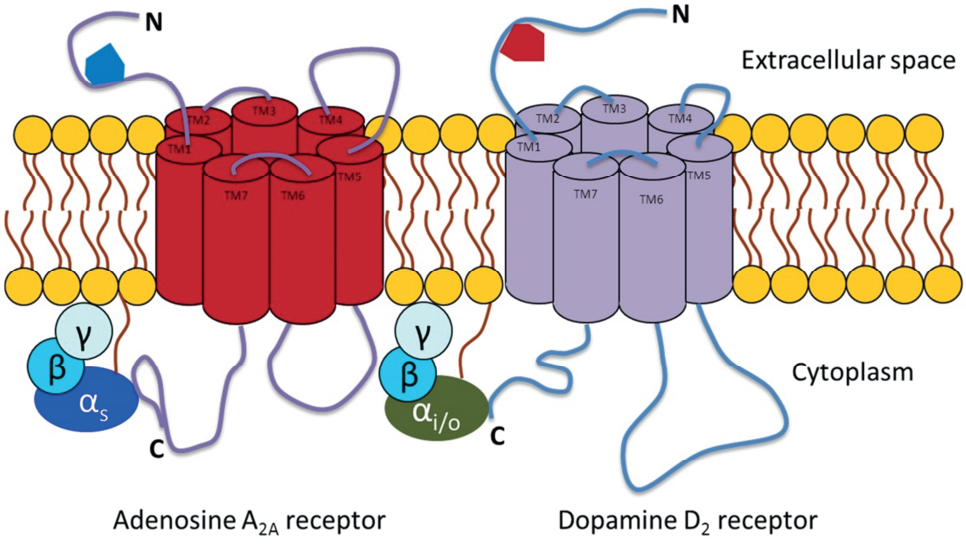


**Figure 1.1** Colocalization of adenosine $A_{2A}$ receptor with dopamine $D_2$ receptor.

change of the other receptor (heteromer partner), resulting in reduced affinity of the heteromer partner towards its ligands. This allosteric interaction of the $A_{2A}R$-$D_2R$ heteromer modulates neuronal excitability and neurotransmitter release. $A_{2A}Rs$ that do not form heteromers with $D_2Rs$ interact with $D_2Rs$ at the AC level via G-protein-dependent pathways, with their AC-signaling suppressed by tonic inhibition via $D_2Rs$ which are negatively coupled to AC [13]. The $A_{2A}R$-$D_2R$ interaction plays an important role in basal ganglia disorders, such as PD [10], Huntington's disease (HD) [14] and depression [15].

Furthermore, about 23% of $A_{2A}Rs$ are localized presynaptically [16], where they form functional heteromers with $A_1R$ (**Figure 1.2**). Presynaptic $A_{2A}Rs$ are thought to be involved in controlling excitatory glutamate release (glutamate is an important neurotransmitter which controls neuronal activation) at direct basal ganglia pathway [13,17]. The pharmacological importance of this population of $A_{2A}R$ is unclear, but antagonists which are able to target presynaptic $A_{2A}Rs$ were suggested as treatment for dyskinetic disorders such as HD and levodopa-induced dyskinesia [17]. In extra-striatal regions, $A_{2A}Rs$ are expressed mostly at presynaptic terminals, with 20 times lower density than the density in striatum [18]. This small population of $A_{2A}R$ is suggested to have an opposite function as postsynaptic $A_{2A}R$ [19].

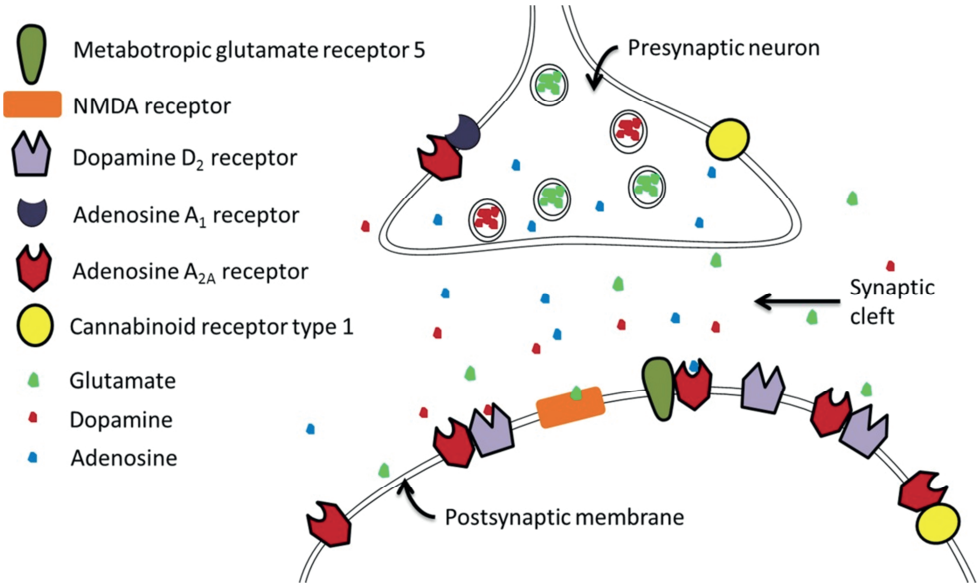


**Figure 1.2** Distribution of striatal $A_{2A}$ receptors in the synaptic region of medium spiny neurons. $A_{2A}Rs$ are colocalized with dopamine $D_2$ receptors, adenosine $A_1$ receptors, cannabinoid receptor 1, and metabotropic glutamate receptor 5, regulating dopaminergic and glutamatergic pathways.

$A_{2A}R$ expression on microglia cells and astrocytes is low under physiological conditions, but can be dramatically increased by brain insults [20], like injury, inflammation, etc.. $A_{2A}R$ regulates microglial activation and proliferation, and also modulates neurotransmission via glial-neuron interaction. With the increasing understanding of glial cells in brain function, especially the role of glial cells in neuroinflammation, $A_{2A}R$ is also studied as a potential therapeutic target to suppress immune response and to protect neurons by antagonizing its activity. The neuronal protective role of $A_{2A}R$ antagonism in several brain disorders [20-22] is now considered to be associated with $A_{2A}R$ situated on glial cells.

**Targeting adenosine $A_{2A}$ receptors in brain disorders**

As we have discussed above, there are two major roles of $A_{2A}R$ in the CNS: locomotor activity regulation and neuroprotection. $A_{2A}R$ antagonism could increase binding affinity of $D_2R$ towards dopamine, and also improve $D_2R$ functioning via an indirect pathway in the basal ganglia (**Figure 1.3**). Locomotor activity is regulated by both the direct and the indirect dopaminergic pathway, the two major circuits in the basal ganglia. $A_{2A}R$ plays an important role in controlling neurotransmission via the indirect pathway and therefore motor symptoms of brain disorders related to disturbed dopaminergic pathways, like PD [10] and HD [23], could be moderated by $A_{2A}R$ antagonism. $A_{2A}R$ antagonism could help to restore the balance between the direct and indirect dopaminergic pathways [10], thus improving motor performance. $A_{2A}R$ antagonism could also be neuroprotective, by suppressing immune responses [20]. Therefore, $A_{2A}R$ is also considered as the target in brain diseases that are not related to dopaminergic dysfunction but suffer from chronic neuroinflammation, like AD. Furthermore, $A_{2A}R$ is also studied as a therapeutic target for psychiatric diseases [24], such as depression [15], schizophrenia [25], and drug addiction [26], because of the antagonistic interaction between $A_{2A}R$ and $D_2R$, and the involvement of $D_2R$ (via dopaminergic pathways, *e.g.,* nigrostriatal pathway (motor control) and mesolimbic pathway (reward control)) in these disorders. However, despite the great potential of $A_{2A}R$ for the treatment of brain disorders, compounds that target $A_{2A}R$ have only been studied in clinical trials as anti-parkinsonism drugs [27]. The investigation of $A_{2A}R$ as a therapeutic target in other brain disorders is still in the preclinical stage. Below are some examples of $A_{2A}R$ as a potential therapeutic target in brain diseases.

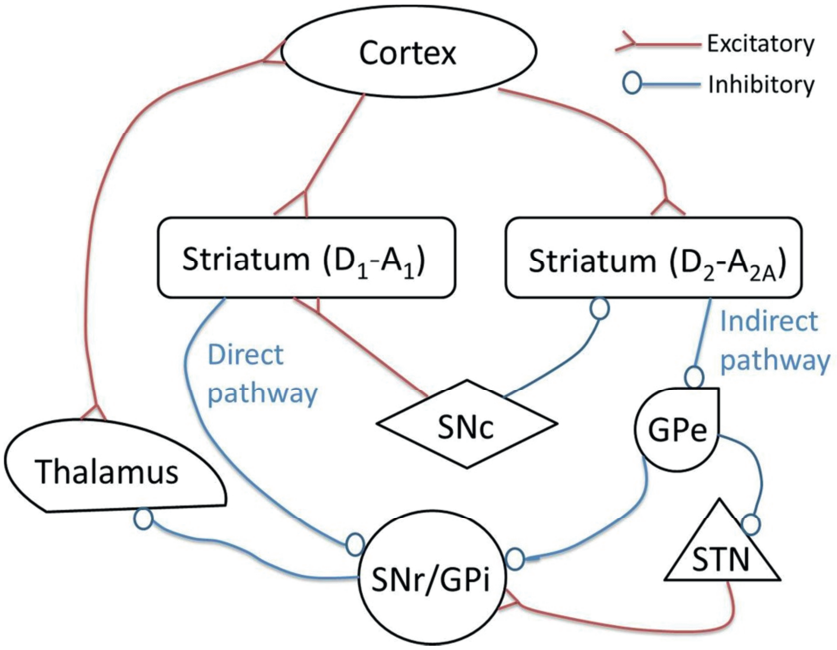


**Figure 1.3** A schematic model of direct and indirect basal ganglia pathways. Dopamine is produced in substantia nigra pars compacta (SNc)) and projected to striatum, acting on stimulation of the $D_1$-$A_1$ receptor heterodimer that is associated with the direct nigrostriatal pathway and on inhibition of the $D_2$-$A_{2A}$ receptor heterodimer that is associated with the indirect pathway. $A_{2A}R$ activation in striatum in the indirect pathway excites the neurons thus attenuates the inhibitory effect (due to $D_2$ receptor activation) on the globus pallidus pars externa (GPe). The death of dopaminergic cells in SNc results in a disturbed balance between the direct and indirect pathways: *i.e.,* attenuation of inhibition of the substantia nigra pars reticulate/globus pallidus pars interna complex (SNr/GPi) via the direct pathway and attenuation of inhibition (GPe-SNr/GPi) and amplification of excitation (subthalamic nucleus (STN)-SNr/GPi) on SNr/GPi via the indirect pathway, leading to remarkable decrease in the output from SNr/GPi to thalamus, resulting in motor deficits as the final outcome.

**Parkinson's disease.** PD is characterized by a deficit in dopamine release in striatum, due to neuronal death in the subtantia nigra, where dopamine is produced. The shortage of dopamine results in the hyperactivity of the indirect basal ganglia pathway and hypoactivity of the direct basal ganglia pathway (**Figure 1.3**). Therefore, hypokinetic symptoms, including shaking, rigidity and slowness of movements occur [28]. In order to restore the dopamine supply, levodopa (levodopa is converted to dopamine in the brain) is given to PD patients as the standard treatment. However, side effects, such as motor fluctuations, dyskinesia, which is characterized by involuntary muscle movements, and an increasing off-time (the period when the drug loses its effect) due to long-term treatment are the major disadvantages of levodopa medication [29]. The excessive dopamine levels produced from levodopa shortly after drug administration are the major cause of levodopa-

induced dyskinesia (LID). $A_{2A}R$ antagonism may facilitate dopamine signaling via the indirect basal ganglia pathway without introducing the motor complications [30]. This could be feasible, because $A_{2A}R$ antagonism can potentiate $D_2R$ functioning without adding extra dopamine burden to the system. KW-6002, an $A_{2A}R$ selective antagonist, was approved for marketing as an anti-Parkinson drug in Japan. Clinical studies of KW-6002 showed that this drug was able to reduce off-time without exacerbating LID [31]. Several other $A_{2A}R$ antagonists, including ST1535, tozadenant (SYN115), V2006, V81444 and PBF509 are under phase I/II clinical trials. These drug candidates are either tested in combination with levodopa, or as monotherapy [27].

**Alzheimer's disease.** AD is the most prevalent neurodegenerative disorder, affecting 6% of people of 65 years or older. AD patients suffer from progressive impairment of memory, as well as other social and body functions, and ultimately, death. Toxic amyloid-β peptide (Aβ) deposits are widely spread in the brain of AD patients, destroying neurons in hippocampus, the region governs memory, and in several cortical regions [32]. An epidemiologic study has suggested that chronic intake of caffeine for 20 years could significantly reduce the risk for AD [33]. AD animal models have shown that treatment with $A_{2A}R$ antagonists reduced synaptic loss and neuronal death triggered by Aβ aggregation. Both acute and long-term treatment with caffeine reduced Aβ levels in the brain of Aβ transgenic mice and alleviated cognitive deficits [21,34,35]. The beneficial effects of $A_{2A}R$ antagonism might be due to the suppression of neuroinflammation by glial cell expressing $A_{2A}R$, inhibition of excitatory glutamate release by presynaptic $A_{2A}R$, or restoration of impaired long-term synaptic potentiation by postsynaptic $A_{2A}R$ [36]. $A_{2A}R$ antagonism also seems to affect Aβ cleavage, but the underlying mechanism has not yet been understood.

**Schizophrenia.** Schizophrenia is a psychiatric disorder, in which dopaminergic and glutamatergic neurotransmission is disturbed [37]. Schizophrenia was also found to be associated with neuroinflammation [6,38]. Because of the regulatory role in dopaminergic and glutaminergic neurotransmission and in neuroinflammation, $A_{2A}R$ has attracted attention for the treatment of schizophrenia [25]. Post-mortem studies on schizophrenic patients showed an elevated level of striatal $A_{2A}R$ [39]. Furthermore, transgenic animal models suggested that a reduction in adenosine level or loss of function of $A_{2A}R$ may be associated with schizophrenic like behavior [40]. These findings imply that $A_{2A}R$ may be a potential target for the treatment of schizophrenia.

## Adenosine $A_{2A}$ receptor as the diagnostic target in brain disorders

As we have discussed before, $A_{2A}R$ plays an important role in many brain disorders associated with neuroinflammation or/and impaired dopaminergic/glutamatergic pathways. Therefore, it would be worthwhile to explore $A_{2A}R$ as a diagnostic biomarker for brain disorders with altered $A_{2A}R$ expression. To be a good diagnostic biomarker, $A_{2A}R$ should be able to 1) identify a particular disease, preferably before clinical symptoms appear, and 2) indicate the severity of a disease and 3) allow monitoring disease progression and response to treatment. *In vivo* imaging methods could be applied to quantify $A_{2A}Rs$ in the brain under various pathological conditions. In order to visualize $A_{2A}R$ in living subjects, small compounds, with high affinity and selectivity to $A_{2A}R$, and proper lipophilicity (octanol water partition coefficient at pH7.4 ($LogD_{7.4}$) between 2 and 4) could be labeled with radioisotopes and administered to animals or human subjects. A powerful technique for measuring the distribution and the amount of target molecule (*e.g.,* $A_{2A}R$) by tracking radionuclides in living subjects is positron-emission tomography (PET).

## POSITRON EMISSION TOMOGRAPHY

PET is an *in vivo* 3-dimensional (3D) imaging technique which allows measuring of biochemical parameters by detecting pharmaceuticals labeled with positron-emitting radionuclides. A positron is the antiparticle of an electron, with the same mass as an electron, but with an electric charge of +1e. Radioactively labeled pharmaceuticals are called radiopharmaceuticals, tracers, or radioligands. After administration of a tracer to a living subject and distribution over the body, the tracer is engaged in the specific biological process of interest and accumulates at its target site. When a positron is emitted from a positron-emitting radionuclide, it travels a short distance, usually 0-3 mm, depending on the kinetic energy of the positron and the density of the medium. While traveling through tissue, the positron loses its kinetic energy by interacting with surrounding electrons. Finally, the positron hits an electron and the two particles annihilate, converting their mass into two gamma photons traveling in opposite directions ($180^o$ angle if the kinetic energy of the electron-positron pair at the time of annihilation is zero, but slightly deviating from the $180^o$ angle if some kinetic energy remains at the time of annihilation). Based on Einstein's mass-energy equation $E = mc^2$, the mass of a positron and an electron is converted into two gamma photons with an energy of

511 keV each. The two photons are subsequently detected by a PET camera. The PET camera will only register the event, when two photons with an appropriate energy are detected within a small time window (coincidence detection). The place where the annihilation happened can be localized by measuring a certain amount of photon pairs that are produced in the same region. Then the signal is analyzed to obtain information on the distribution, the density, or the biological process of the target molecule in tissue (**Figure 1.4**). $^{15}O$, $^{13}N$, $^{11}C$, $^{18}F$, $^{64}Cu$ and $^{89}Zr$ are commonly used positron emitting radionuclides, with half-lives of 2.0, 10.0, 20.3, 109.8 min, and 12.7 and 78.4 h, respectively. Recently, $^{68}Ga$ and $^{82}Rb$ attracted increasing attention because generators to produce these isotopes became commercially available. $^{15}O$, $^{13}N$, and $^{11}C$ have very short half-lives, therefore, an on-site cyclotron is required to produce these isotopes. The advantages of short-lived radionuclides over long-lived radionuclides include 1) multiple scans can be applied in the same subject in a short period of time (*i.e.,* within one day); 2) low ionizing radiation burden for patients (ionizing radiation is a radiation that carries high energy that is able to ionize molecule inside our body, gamma rays and X-rays

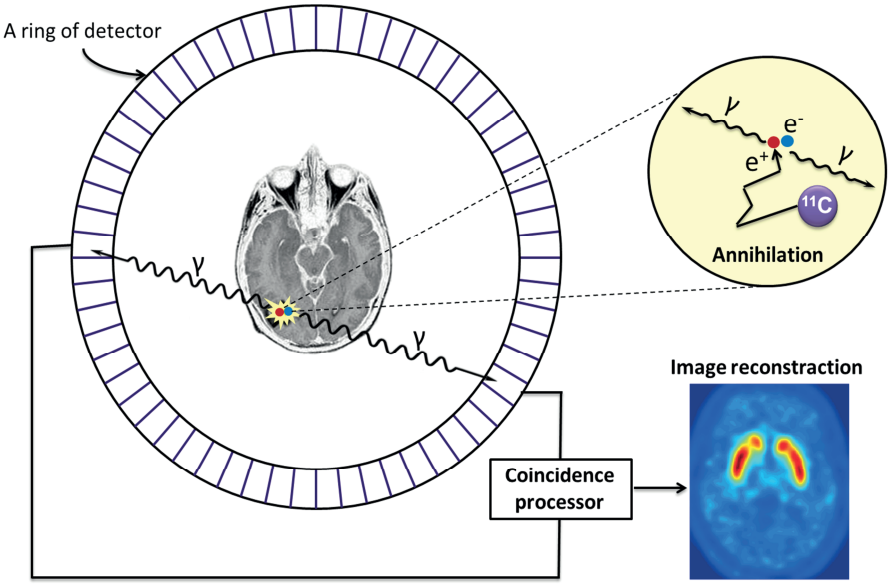


**Figure 1.4** Schematic illustration of the basics of PET. A positron ($e^+$) is emitted from the radioligand and annihilates with an electron. A pair of gamma photons traveling in opposite directions are generated. The detector crystal of a PET camera registers the event when two photons are detected in coincidence. Two detector crystals have to detect a 511 keV gamma ray but this event is only recorded when detection occurs within a short coincidence time window. Then the number and the distribution of the coincidences are analyzed. The PET data are finally reconstructed into images.

are examples of ionizing radiation); 3) these radionuclides can be used for labeling endogenous molecules. Isotopes with long half-lives have the advantage that radiopharmaceuticals labeled with these isotopes can be distributed from the cyclotron to peripheral PET centers without a cyclotron. In addition, long half-life isotopes allow scanning after a long distribution time of the tracer (*e.g.,* more than one hour). This is useful to quantify the kinetics of tracers with long biological half-lives. For molecules which have very long serum half-lives, *e.g.,* antibodies, labeling these molecules with long half-life isotopes, *e.g.,* $^{89}$Zr with a half-life of 78.4 h, allows to scan subjects a few days after tracer administration when there is sufficient amount of radioligands penetrating the tissue to reach the target and sufficient clearance of unbound tracer.

## PET RADIONUCLIDE PRODUCTION

At the Department of Nuclear Medicine and Molecular Imaging (NMMI) of the UMCG, $^{15}$O, $^{13}$N, $^{11}$C, and $^{18}$F are produced by an IBA-18 cyclotron (**Figure 1.5A**). In the ion source at the center of the cyclotron, $H_2$ gas is broken down into $H^+$ (proton) and $H^-$. $H^-$ is pulled out and accelerated by a high frequency alternating voltage, and its motion is bend into a curved trajectory by a perpendicular magnetic field. The $H^-$ speeds up each time it crosses the electrical field between a Dee and a sector at ground potential (*i.e.,* 4 accelerations per turn). Because of the acceleration, the kinetic energy is increasing gradually and the perpendicular magnetic field causes $H^-$ to travel in a spiraling horizontal path. Finally, at the edge of the cyclotron, two electrons are stripped from the $H^-$ when it goes through a carbon foil. Then the $H^+$ particle is directed to a target filled with specific molecules. Protons produced by the cyclotron collide with the nuclei of the target molecules to generate positron emitting nuclides (**Figure 1.5B**). For instance, $^{11}$C is produced by interacting protons with $^{14}N_2$, and $^{18}$F can be produced by $^{18}$O-proton collision. Then the resulting radionuclides are released from the target to the site of radiolabeling.

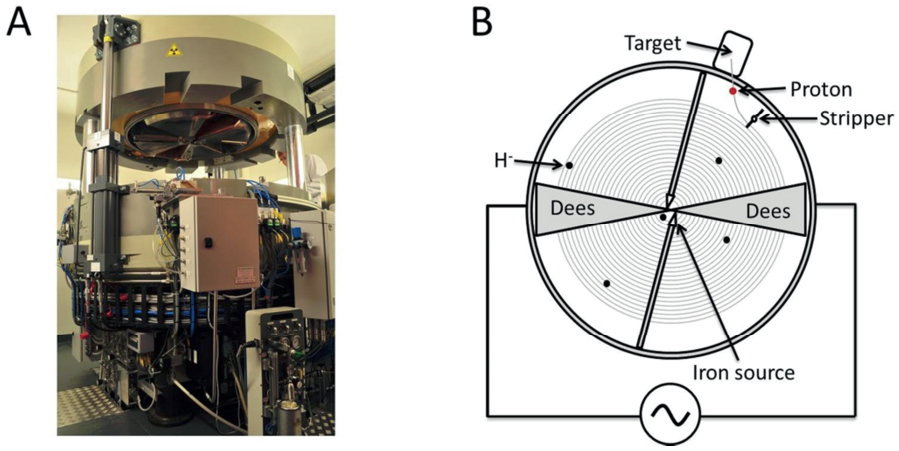


**Figure 1.5** (**A**) An IBA-18 cyclotron (open). (**B**) Inside the cyclotron (a top view). Dees are electrodes with alternating electrical fields. $H^-$ is produced in an ion source at the center of the cyclotron. $H^-$ speeds up as traveling from the center to the edge in a spiral path, and the two electrons of the $H^-$ are stripped by a foil stripper at the end of its journey. A proton ($H^+$) is produced. The proton is guided to the target to react with molecules in the target to generate radionuclides.

## PET Tracer synthesis

After transport to the site of radiolabeling, the radionuclide is allowed to react chemically with a precursor to form a tracer. Fast reactions are crucial for labeling of radioligands with short half-life isotopes, like $^{13}N$ and $^{11}C$. For $^{11}C$ tracers, the final product should be obtained within 60 min (3 half-lives of $^{11}C$), because the radioactivity and specific activity (specific activity is the amount of radioactivity per mass unit of the tracer) at 60 min have decreased to 1/8 of the value at the beginning of the synthesis. In order to guarantee enough radioactivity at the end of the synthesis, high amounts of radioactivity at the start of synthesis are required. Therefore, the radiosynthesis is commonly conducted inside a hotcell with lead walls and doors to provide shielding. The synthesis can be performed with an automated robotic system or synthesis module to reduce the radiation burden to the operator (**Figure 1.6**). A large excess of labeling precursor (a few hundred-thousand times more precursor than the radionuclide) is used to create pseudo-first-order reaction kinetics. In this situation, the rate of reaction is maximum with respect to the radionuclide. When the reaction is done (usually within 10 min for $^{11}C$-labeled radiopharmaceuticals, no full conversion is needed), the reaction mixture is usually purified and formulated. The specific activity of the final product is measured before tracer administration. The specific activity and the

injected amount of radioactivity determine the injected mass of the tracer. The injected mass should be kept as low as possible (especially in studies in small animals) to avoid saturation of the target receptor, transporter or enzyme. Therefore, for $^{11}C$ labeling, [$^{12}C$]$O_2$ or [$^{12}C$]$H_4$ should be removed as much as possible from tubings and reactors as [$^{12}C$]$O_2$ and [$^{12}C$]$H_4$ contaminate [$^{11}C$]$O_2$ and [$^{11}C$]$H_4$ produced by the cyclotron. Even with strategies such as flushing lines with inert gas, the amount of [$^{12}C$]$O_2$ and [$^{12}C$]$H_4$ is still hundreds to thousands times more than [$^{11}C$]$O_2$ and [$^{11}C$]$H_4$ in the reaction system. Together with the decay during the synthesis, the specific activity of $^{11}C$ tracers is normally tens to a few hundred GBq/μmol. $^{18}F$-labeled tracers are usually obtained with a few times higher specific activity than $^{11}C$ tracers, as it is easier to avoid contamination of $^{18}F$ with $^{19}F$. For tracers which have low affinity to the target molecules (*e.g.,* a $K_d$ of >10 nanomolar) and a low specific activity at the time of injection, the amount of unlabeled tracer might have already saturated or occupied a substantial amount of the binding sites at a standard injection dose, resulting in a reduced or depleted PET signal. As a rule of thumb, less than 5% of the target molecule should be occupied by a tracer [41], in order to consider the physiological condition as unchanged.

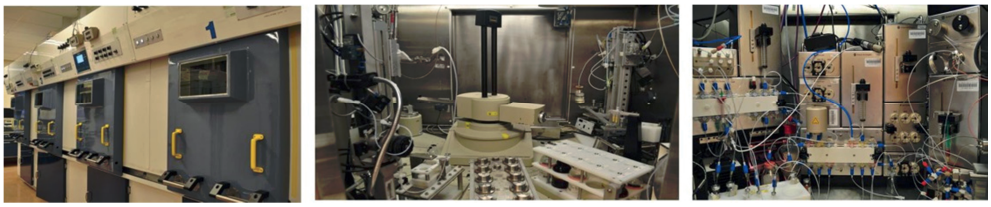

**Figure 1.6** Hotcells (left), an automated robotic system (middle), and synthesis modules (right) inside a hotcell.

### *$^{11}C$ tracers*

$^{11}C$ has the same chemical properties as $^{12}C$, therefore, the biological properties of a $^{11}C$ compound are identical to its $^{12}C$ analogue. This could be an advantage for the *in vivo* assessment of the properties of pharmaceuticals during the drug development and for the study of the behavior of endogenous molecules. For $^{11}C$ tracer production, [$^{11}C$]$H_3I$ and [$^{11}C$]$H_3OTf$ are frequently used radioactive synthons. They react with the labeling precursor via a $S_N2$ mechanism [42]. The precursors should contain a nucleophilic group. Oxygen from a hydroxyl group and

nitrogen from amino groups are examples of such nucleophiles. Other strategies can also incorporate $^{11}C$ to a chemical compound, for example, [$^{11}C$]O and [$^{11}C$]$O_2$ insertion to form aldehydes, ketones, ethers, amides, acids, etc. [43,44], but these methods are not so well established yet.

### *$^{18}F$ tracers*

$^{18}F$ is the most popular radionuclide for PET imaging nowadays, because of the suitable half-life and high specific activity of the resulting radioligands. $^{18}F$-fluo-2-rodeoxy-D-glucose (FDG) is the mostly commonly used PET tracer, especially in cancer diagnosis, which occupies ~90% of the PET scans worldwide [45]. Isotropic radiolabeling of $^{18}F$ is limited because $^{19}F$ is not so frequently present as $^{12}C$ in natural compounds, although fluoride atoms are regularly present in drugs. However, the fluoro group is similar to a hydroxyl group in terms electronegativity. Therefore, $^{18}F$ analogues of natural compounds are synthesized by replacing a hydroxyl group from the parent compound with fluorine-18. Fluorine-18 is also used to substitute other atoms, like halogens or hydrogen atoms. However, we should keep in mind that there is a slight difference between –F and these other atoms and therefore the biological properties of the $^{18}F$ analogues are not identical to their parent compounds.

### Requirements for radioligands for receptor imaging

The criteria for suitable radioligands should aim to achieve that the measured radioactive signal reflects the underlying process of interest.

The most important criterion for a PET radioligand targeting an endogenous molecule is a sufficiently high affinity of the tracer towards the target. The dissociation constant $K_d$ is the commonly used parameter to measure the affinity, which is obtained from the following equation: $K_d = [L]*[R]/[LR]$, where [L] is the concentration of the unbound ligand, [R] is the concentration of the unbound receptor (target molecule), and [LR] is the concentration of the ligand-receptor complex in the reaction system [46]. $K_d$ is difined as the concentration of the free ligand L at which half of the total receptor R forms a complex with L. A small $K_d$ indicates high affinity of L to R. $K_d$ can be predicted by *in vitro* competition binding assays when the system is at the steady state (*i.e.,* [L], [R], and [LR] are constant at any time point). A good radioligand usually has a $K_d$ value in the picomolar to nanomolar range [47]. However, a radioligand with too high affinity is not ideal, because this could result in difficulties in quantification of tracer kinetics

(inaccurate estimation of several rate parameters, *e.g.,* $k_3$ and $k_4$, see section 'TRACER QUANTIFICATION-KINETIC MODELING' for explanations of these parameters) for reversible tracers, and loss of sensitivity to detect changes of target molecule for irreversible tracers. Furthermore, hours of scan duration is uncomfortable for patients and logistically unpractical.

Secondly, the metabolism of radioligands should not be too fast. Fast metabolism would reduce the number of radioligands reaching the target, lowering the signal from target regions. Furthermore, fast metabolism may cause problems for tracer quantification, since radiometabolite(s) contribute to the background and can also contribute to the specific signal in target regions, provided that the metabolite(s) have affinity to the target molecule, egress the blood vessel and, in case of brain imaging, penetrate the blood-brain barrier (BBB). Pharmacokinetic modeling could be applied to subtract the contribution of radioactive metabolite(s) from the total signal. However, such calculation is sometimes erroneous and can be highly variable because of the difficulty of measuring/estimating the amount of radioactive metabolite(s) in the target region.

Thirdly, high selectivity to the target is required for radioligands. A tracer should not only bind to the target, but should bind to it exclusively. Many target molecules in our body have analogues with similar structures. For example, $A_{2A}R$ shares 50% gene sequence homology with $A_3R$. Radioligands for $A_{2A}R$ should not bind to $A_3R$ or vice versa, because the non-selective binding would increase the signal in target regions where the two receptors coexist, resulting in erroneous quantification of the target molecule. Furthermore, it is inevitable that tracers bind to tissue non-specifically (binding to tissues and/or some unknown endogenous molecules. Such binding cannot be displaced), and sometimes non-selectively (specific binding to another target). However, such binding should be kept to minimum.

In addition, radioligands should not be the substrate of an ATP-dependent drug efflux pump, such as P-glycoprotein 1, unless that the efflux pump is the target of the radioligand. The pump proteins exist at the membrane of many cells, actively transport their substrates from the inside of the cells to the outside, resulting in a low accumulation of ligands in target regions. For radioligands targeting the CNS, a few more issues should be taken into consideration because of the BBB. This brain guardian protects the CNS from toxins, bacteria, and other insults, but it also prevents almost 100% of the large molecule and 98% of the small molecule CNS drug candidates from entering the brain [48]. Radiolabeled antibodies, which are

frequently used for the imaging of the peripheral targets, are usually out of consideration for brain imaging, because these molecules are too big to enter the brain. Actually, compounds with molecular weight above 500 Da may have difficulty penetrating the BBB. Tracers travel across the BBB through either passive diffusion or active transport. In case of active transport, the tracer is transported into the brain via specific transporters at the BBB (*e.g.,* $^{18}$F-FDG via GLUT-1). This transporter-mediated molecule delivery allows the entry of macromolecules (*e.g.,* antibodies) into the CNS when the molecule is fused to a substrate of a transporter expressed at the BBB. The first successful application of this strategy to deliver PET tracers to the brain was reported by Sehlin et al. [49] in 2016. In case of passive diffusion, the tracer should be lipophilic, because of the lipophilic nature of the BBB. However, the molecule should not be too lipophilic, otherwise it binds non-specifically to lipophilic targets, like plasma proteins and the cell membrane. Therefore, CNS targeting radioligands normally have a $LogD_{7.4}$ in the range 2-4. Finally, in brain imaging studies, the penetration of peripherally produced radioactive metabolites into the brain should be very limited, and the contribution of the signal from all radioactive metabolites (periphery- and/or CNS-produced) in the brain should be small (*i.e.,* less than 10% of the total signal), or should be corrected for.

**PET tracers for adenosine $A_{2A}$ receptors**

A good $A_{2A}$R tracer could help to acquire a better understanding on the distribution, density and the biological roles of $A_{2A}$Rs. Furthermore, $A_{2A}$R-PET could be a useful tool to assess drug candidates targeting $A_{2A}$R during drug development and can be applied as a diagnostic or staging tool to monitor $A_{2A}$R changes during the disease courses. We learned from our previous discussion that the criteria for CNS radioligand selection are rather strict. For this reason, only a few radioligands are available so far for $A_{2A}$R imaging. Four $A_{2A}$R radioligands (**Figure 1.7**) have been tested in humans and 2 of them were used to study the $A_{2A}$R availability in PD and Multiple Sclerosis (MS) patients [50-57]. Differences in $A_{2A}$R density were observed between MS patients and healthy volunteers ([$^{11}$C]TMSX-PET) and between PD patients with LID and healthy volunteers/drug naïve PD patients ([$^{11}$C]TMSX-PET and [$^{11}$C]SCH 442616-PET). However, due to the unsatisfactory properties of these radioligands, like low brain uptake and lack of specificity, the sensitivity of the technique was low and the interpretation of experimental observations was difficult. A new $^{18}$F labeled radioligand [$^{18}$F]MNI-444 was first reported in 2014 [58]. In 2015 the first human study was reported with

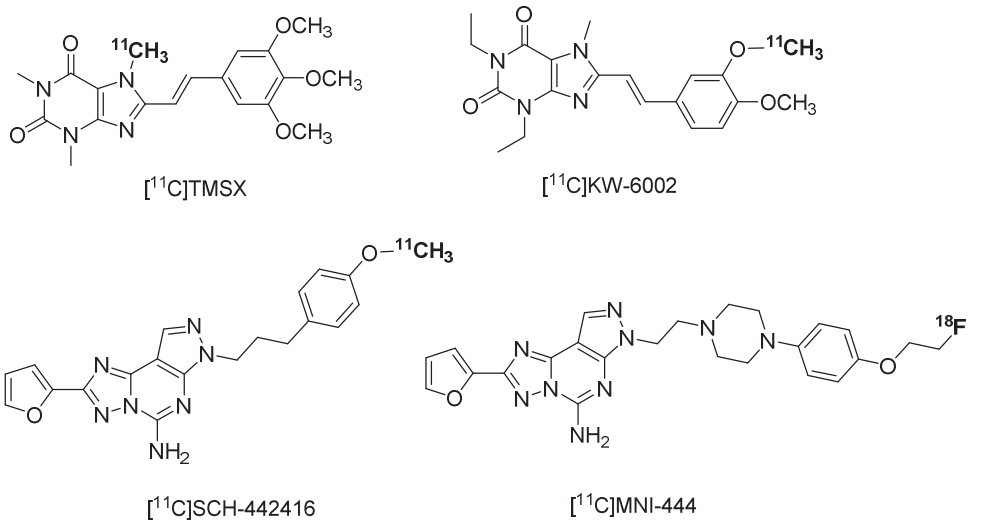


**Figure 1.7** $A_{2A}R$ PET imaging radioligands that have been tested in human subjects.

this radioligand [50]. This tracer displayed substantially better properties than the previously reported radiopharmaceuticals in terms of high and robust binding potential ($BP_{ND}$) values in striatum and high test-retest reproducibility. However, the slow kinetics of this tracer might be a problem, as at least 1.5-2 h dynamic acquisition is necessary to quantify the tracer kinetics.

## TRACER QUANTIFICATION-KINETIC MODELING

Generally speaking, kinetic modeling is a mathematic description of the kinetic pattern(s) of a specific process. In the field of PET imaging, kinetic modeling is used to quantify biological processes like molecular transport, interactions, and metabolism. This method is mainly applied for tracers targeting receptors in the brain. Therefore, the discussion here will be limited to the kinetic modeling of tracers targeting CNS. In PET studies, the time-activity curves (TACs) of a tracer in regions of interest are obtained from dynamic PET scans. The signal detected by the PET camera is a combination of the signal from the brain parenchyma and the blood compartment. The TAC reflects the total response of the system. In order to quantify the amount of tracer molecules bound to the target and the amount bound to tissues non-specifically or as free molecules in body fluids, kinetic modeling is applied to fit the tracer TACs. Kinetic modeling calculates pharmacokinetic parameters of a tracer as output parameters. Examples of outcome parameters are the rate constants between compartments ($K_1$, $k_2$, $k_3$, $k_4$) when compartment

modeling is applied, the tracer concentration in regions of interest as compared with tracer concentration in plasma (distribution volume: $V_T = C_T/C_P$) or a reference region devoid of target molecule (distribution volume ratio: DVR = $C_T/C_R$), and metabolic rate constant $K_i$. Therefore, the aim of kinetic modeling is to mathematically solve the kinetic parameters of a tracer in tissue in response to an impulse, such as the plasma input function.

Kinetic modeling methods which require the information of tracer concentration in plasma are called invasive modeling methods (**NB.** the plasma activity determines the input function, not the tracer concentration in the whole blood, because the tracer molecules in plasma, but not bound to red blood cells, are freely delivered to tissues). For invasive kinetic modeling, arterial blood samples are taken from the subject during the scan and the activity in plasma and the whole blood is measured with a well counter or a dedicated automated blood sampling device for blood activity measurement. The TAC of the intact tracer in plasma (which is corrected for radioactive metabolites) is used as the input function for tracer TAC fitting in tissues of interest. The activity in the whole blood is used to correct for the signal from the blood vessels by subtracting the activity in fractional blood volume in tissue from the activity in volumes of interest (VOIs) measured by PET. The blood activity could also be measured with dynamic PET imaging on major blood vessels (*e.g.,* carotid artery). But still, plasma-to-blood ratio and tracer metabolic profile have to be obtained with invasive blood sampling.

**Compartment modeling**

Compartment modeling is an invasive modeling method which requires arterial input function. In practice, only two types of compartment modeling methods are commonly used. They are the one-tissue compartment model (1TCM) and the two-tissue compartment model (2TCM) (**Figure 1.8**) [59]. The 1TCM assumes that the tracer goes directly from the plasma to the target. So there are virtually two compartments, the plasma compartment and the tissue compartment. This model calculates the rate constants $K_1$ and $k_2$, which describe the rate of the tracer from plasma to the tissue, and the rate of the tracer from tissue to plasma, respectively. $K_1/k_2$ [59] describes the ratio of the tracer in the tissue to the arterial plasma concentration at an equilibrium and is defined as the distribution volume ($V_T$). The 2TCM assumes that the tracer goes from arterial plasma to the central

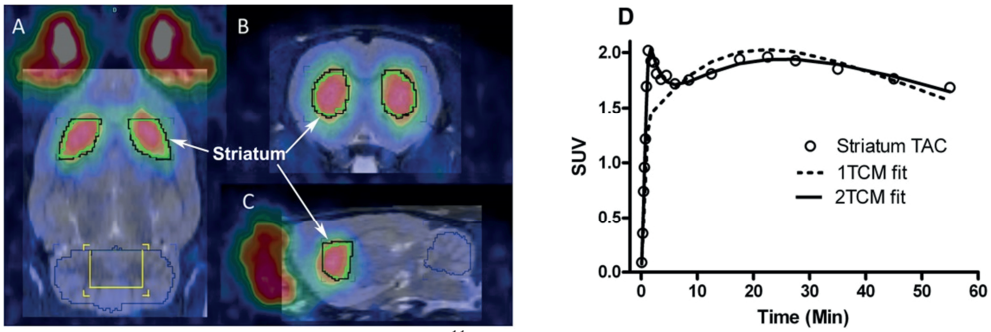


**Figure 1.8** An example of PET-imaging of [$^{11}$C]preladenant (a reversible radioligand for adeonsine $A_{2A}$ receptors) uptake in the rat brain (**A**: top view, **B**: front view, **C**: side view) and model (one-tissue compartment model (1TCM) and two-tissue compartment model (2TCM)) fits of the tracer time activity curve (TAC) in the target region (striatum) (**D**). The hot spots outside the brain in the PET images represent tracer uptake in Harderian glands.

non-displaceable compartment, where part of the tracer molecules bind to the tissue non-specifically and reach the equilibrium rapidly and some molecules retain in the tissue fluid as free ligand. The rest of the ligand is transferred from the non-displaceable compartment to the specific compartment, in which it is bound to the target molecule specifically (**Figure 1.9**). Note that these compartments are not physically separated, they are drawn and described separately for the sake of ease. In case the specific compartment is slow, and therefore distinguishable from the fast non-displaceable compartment, the 2TCM can be used to describe the tracer kinetics. Four parameters, $K_1$, $k_2$, $k_3$ and $k_4$, are calculated by solving the modeling equations by non-linear fitting of the tissue TACs using the arterial plasma input function. $K_1$ and $k_2$ indicate the rate of the tracer from plasma to the non-displaceable compartment, and the rate of the tracer from the non-displaceable compartment to plasma, respectively. $k_3$ reflects the rate of the tracer from the non-displaceable compartment to the specific compartment, and $k_4$ describes the rate of the tracer from the specific compartment to the non-displaceable compartment. The $V_T$ can be obtained from the modeling parameters using the equation $K_1*(1+k_3/k_4)/k_2$ [59]. Another kinetic parameter derived from the reversible 2TCM fit is the non-displaceable binding potential $BP_{ND}$, which is the ratio of $k_3$ and $k_4$ [59]. $BP_{ND}$ indicates how well the tracer binds specifically to the target. $BP_{ND}$ also reflects the ratio between the density of target molecule ($B_{max}$) and dissociation constant $K_d$ of the tracer/target complex at an equilibrium when the concentration of the free ligand is much smaller than $K_d$ (at a tracer dose). Individual values of $B_{max}$ and $K_d$ cannot be obtained from a single PET scan with bolus injection, but only the ratio of them ($BP_{ND}$). A Schatchard plot with multiple scans (at least 2

scans) with specific activities ranging from low to high using a bolus + infusion protocol is the commonly used strategy to calculate $B_{max}$ and $K_d$ individually [60,61].

In case tracer molecules are trapped in the specific compartment, the $k_4$ is equal to or approaches zero. $^{18}$F-FDG is a typical example of an irreversibly bound tracer. The most important pharmacokinetic parameter that can be obtained from an irreversible 2TCM fit is the metabolic rate $K_i$, calculated as $K_i = K_1 * k_3 * / (k_2 + k_3)$ [62].

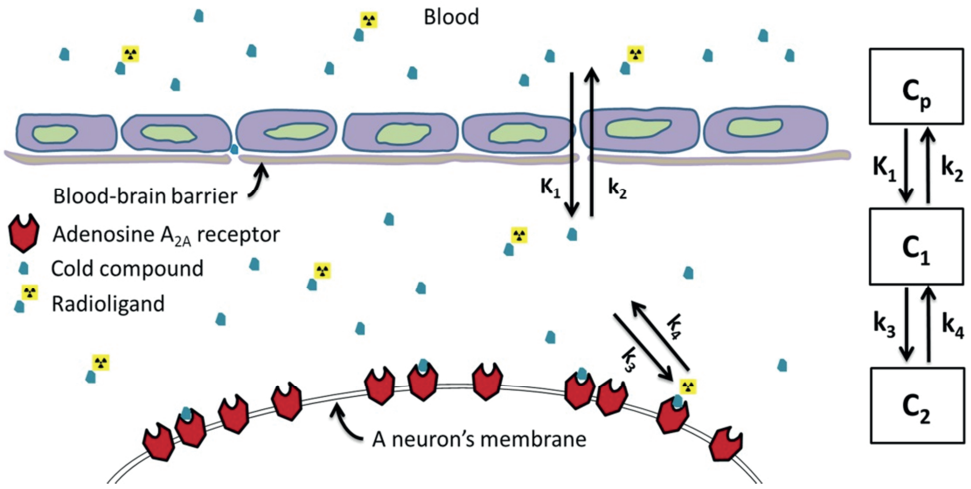


**Figure 1.9** An illustration of a reversible two-tissue compartment model with tracer concentration in plasma ($C_p$), the non-displaceable compartment ($C_1$), and the specific compartment ($C_2$). The $K_1$-$k_4$ are rate constants between these compartments.

## Graphical analysis: Logan plot and Patlak plot

Logan [63] and Patlak [62] graphical analysis are two of the most frequently used methods to calculate $V_T$ for reversibly binding tracers, and $K_i$ for irreversibly binding tracers, respectively, using linearisation approaches. An example of a Logan plot is presented in **Figure 1.10**. These graphical analysis methods require a plasma input function. Compared with compartment modeling, which calculates micro-parameters (*e.g.,* $K_1$, $k_2$, $k_3$, and $k_4$), graphical analysis obtains macro kinetic parameters ($V_T$, $K_i$) in a simple way. The parameters obtained from graphical analysis are usually more robust than parameters derived from compartment models. Furthermore, graphical analysis is model-independent. If tracers fail to have a good convergence with compartment model fits, graphical analysis could be explored to obtain $V_T$ or $K_i$. However, graphical analysis uses several assumptions, such as the operational equations of these methods require that some time after tracer injection, which is defined as $t^*$, the system reaches its steady state: *i.e.,* the

activity concentration in tissue divided by activity concentration in plasma becomes time-independent. Furthermore, Logan graphical analysis requires that $k_2 << k_4$. In case of violation, the plot becomes linear at later time points and the $V_T$ is underestimated. In addition, graphical analysis ignores the blood compartment in tissue and is sensitive to data noise. These restrictions can lead to a negative bias in $V_T$ and $K_i$ estimations [64]. Nonetheless in practice, graphical analysis methods work quite well even with violation of underlying assumptions and with noisy data (*e.g.,* 10% average noise). $V_T$ or $K_i$ obtained from graphical analysis are usually quite comparable with the parameters derived from compartment model fits. For example, in case of data from **Figure 1.10**, $k_2$ was calculated larger than $k_4$ by 2TCM fits, and the tissue-to-plasma activity ratio increases over time at later times. However if we look at **Figure 1.10B**, the data points approach linearity much earlier than 90 min (the $t^*$ was set to 22 min), indicating that the system approximately reaches a steady state (time-dependent changes become sufficiently slow) before tissue-to-plasma ratio becoming constant. As a result, the underestimation of $V_T$ with Logan plot as compared with 2TCM fit was only 3%.

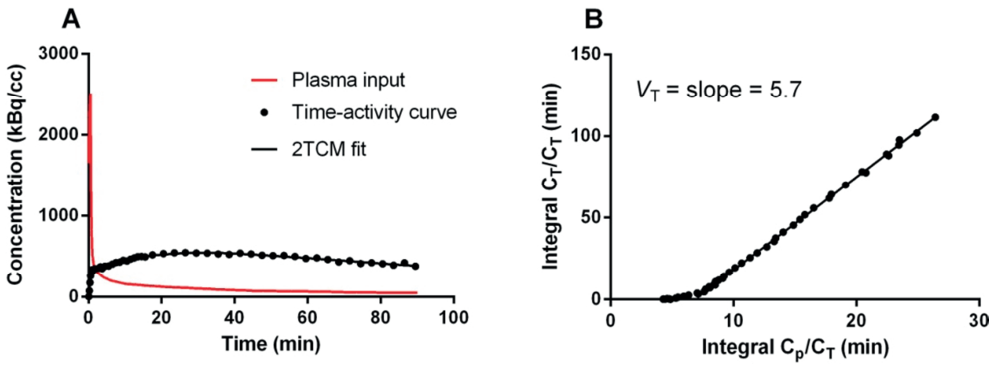


**Figure 1.10** (**A**) Plasma input function and the time-activity curve (TAC) of [$^{11}$C]preladenant (a reversible radioligand for adeonsine $A_{2A}$ receptors) uptake in striatum in the monkey brain. The TAC is fitted with the two-tissue compartment model (2TCM) using non-linear regression. (**B**) Linear regression of the striatum-plasma system using Logan graphical analysis ($t^*$ = 22 min). The slope of the regression is equal to $V_T$. For tracers described by a one-tissue compartment model (1TCM), the straight line starts from the beginning. For tracers which cannot be well-described by a 1TCM, the linear portion starts at $t^*$.

## Reference tissue-based models/methods

Reference tissue methods, in contrast to invasive methods, do not use the plasma tracer concentration, but use the tracer concentration in a reference tissue (measured by PET) devoid of tracer binding sites as an input function. Normally, kinetic modeling with a plasma input function is considered the gold standard for

quantification of tracer kinetics, because plasma is the direct driving force of tissue uptake. Therefore, modeling tracer TACs with plasma input function is theoretically the most proper way to obtain the physiologically meaningful solution. In practice, however, non-invasive reference tissue-based modeling methods that do not require blood sampling are used as an alternative, because of the discomfort of blood sampling, failure of the model fits, or the high variability in pharmacokinetic outcome parameters. These modeling methods are based on several assumptions and simplifications and provide restricted information on tracer kinetics (*e.g.,* distribution volume ratio DVR). In many situations, reference tissue-based methods work surprisingly well. The kinetic parameters predicted by these modeling methods correlate well with the parameters obtained from invasive modeling methods, regardless of many violations to the assumptions on reference tissue-based methods.

The simplified reference tissue model (SRTM) [65], multilinear reference tissue model (MRTM) [66] and reference tissue Logan plot (RLogan) [67] are examples of reference tissue-based models/methods (**Figure 1.11**). Each model/method has its own assumptions and restrictions. Therefore, model/method selection should be based on the kinetic properties of the tracer and reference tissue-based modeling

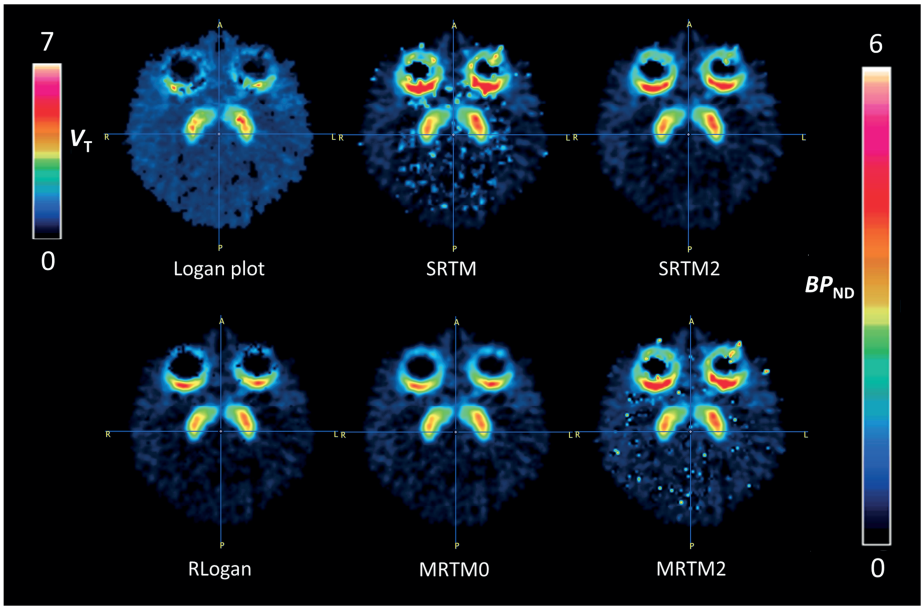


**Figure 1.11** [$^{11}$C]Preladenant parametric images of $V_T$ derived from Logan plot and $BP_{ND}$ obtained from reference tissue-based modeling methods (SRTMs, RLogan, and MRTMs) from a monkey brain. Note that there are many "hot spots" inside the brain with SRTM and MRTM2 fits. These spots are artifacts representing extreme values. Therefore, SRTM and MRTM2 might not be proper modeling methods in this case.

methods should always be validated against invasive compartment modeling or graphical analysis methods. The biggest advantage of a reference tissue based model/method is that blood sampling can be omitted. Not only can the invasive and laborious sampling procedure be avoided, but also the variability due to the blood sampling can be reduced. Reference tissue input function is more stable than arterial input function in most cases. Therefore, reference tissue-based modeling methods could provide more robust macro pharmacokinetic parameters (*e.g.,* $R_1$, DVR and $BP_{ND}$), compared with invasive modeling methods. However, because of the simplifications in the calculation, there are rules for these methods. Violation of the rules can result in a bias as a tradeoff with the reduced variability. Reference tissue-based modeling methods are commonly used, regardless of the violations, if the analyst thinks that the bias is acceptable, or if the bias appears as a scaling factor. Actually, reference tissue based modeling methods were also tested in cases where no receptor-free anatomical region is available. For example, imaging of the translocator protein 18 kDa (TSPO) in the brain. TSPO is widely distributed in the brain so that a region completely devoid of TSPO cannot be defined. Several reference tissue approaches have been tested to obtain $BP_{ND}$, using cerebellum as reference region [68] or extracting reference voxels using cluster analysis [69,70]. In this case, the absolute $BP_{ND}$ value is less important than the variability and reproducibility of the selected method and the ability to differentiate the disease conditions from healthy controls. Again, $BP_{ND}$ could be greatly biased in such cases, but as long as the reference tissue-based methods are sensitive enough to detect changes of target molecule with high test-retest reproducibility and the amount of target molecules in the reference tissue is not different between conditions, the bias can be well tolerated.

**Kinetic modeling *vs.* standardized uptake value**

The standardized uptake value (SUV) is a simple semi-quantitative parameter describing tracer uptake in the tissue. SUV is the most commonly used parameter for clinical studies, *e.g.,* for $^{18}$F-FDG imaging analysis in cancer patient studies. The SUV is defined as the activity concentration in tissue (in MBq/kg or kBq/g) divided by the injected dose (in MBq or kBq), then multiplied by the body weight (in kg or g) or the body surface area ($m^2$) [71,72]. SUV calculation does not require blood sampling. For $^{18}$F-FDG studies, static scans are often acquired some time after tracer administration to obtain SUVs in regions of interest. SUV is able to answer questions such as: where is the glucose being metabolized? Where is a receptor localized? SUV is useful to localize tumors, staging and monitor of

treatment efficacy. However, for comparison between subjects, SUV is less robust, because tracer uptake is not necessarily linear to the body weight and body surface area, and the tracer concentration in plasma and the blood flow might be different between patients. These variables are not considered by SUV analysis but would certainly affect SUVs. Furthermore, SUV is vulnerable to the image noise. To reduce the variability of the SUV data between subjects and the SUVs of same subjects between scans, and also to make multicenter trials comparable, $^{18}$F-FDG PET standardization guidelines were proposed [73-75].

When a dynamic scan is acquired for the kinetic modeling, however, many additional questions can be resolved, like what is the density of a receptor in the tissue? What is the trapping rate of an endogenous molecule to a tissue? How many receptors are occupied after drug administration? How does the blood flow affect an endogenous molecule or drug accumulation in the brain? How does a disease affect the expression of a receptor? Furthermore, kinetic parameters such as $V_T$ and $BP_{ND}$ are more robust and accurate than SUV to quantify tracer uptake in regions of interest, because these parameters are obtained with the consideration of the tracer kinetics in blood or in a reference tissue. On the other hand, kinetic modeling is more laborious than SUV calculation: blood sampling is required in some cases, the dynamic scan is time consuming, and the reconstruction for dynamic images needs more computing power and memory. In addition, kinetic modeling software and personnel with knowledge in kinetic modeling are required to analyze the data. Most importantly, kinetic modeling requires dynamic acquisition so that it cannot provide whole body information (due to limited field of view of the PET camera) which is crucial for cancer and inflammation imaging. Kinetic modeling is frequently used in brain imaging and novel tracer qualification studies, whereas routine clinical PET imaging is normally done with a static scan using either visual analysis or SUV as the outcome parameter. Whether to use SUV or kinetic modeling in a PET study is largely dependent on the research question to be answered, and also on the balance between data robustness and the convenience of patients.

## OUTLINE OF THE THESIS

As discussed previously, the $A_{2A}R$ plays a crucial role in several brain functions. Especially in pathological conditions, like in Parkinson's disease, Alzheimer's disease and schizophrenia, the changes of $A_{2A}R$ have been detected in post-mortem brains. Therefore, it would be very interesting to map the $A_{2A}R$ in the living brain, to unravel the functions of $A_{2A}R$, and to explore it as a therapeutic and diagnostic target in brain diseases.

The aim of this thesis is to develop a novel PET radioligand for the imaging of $A_{2A}Rs$ and evaluate the new tracer in animal models with PET to validate the potency of the tracer for $A_{2A}R$-PET imaging and quantification. The thesis describes the translational studies that enable application of the new tracer in human PET-studies.

**Chapter 2** reports the synthesis and evaluation of a novel $A_{2A}R$ radioligand [$^{11}$C]preladenant in rats. [$^{11}$C]Preladenant is obtained by $^{11}$C labeling of O-demethylated preladenant. The affinity of [$^{11}$C]preladenant to $A_{2A}Rs$ is assessed with *in vitro* autoradiography and *in vivo* PET imaging. Tracer plasma kinetics and the metabolic profile are analyzed. The specific binding of [$^{11}$C]preladenant is studied by PET imaging of the rat brain preblocked with an $A_{2A}R$ subtype selective antagonist KW-6002. Tracer distribution in rats is studied by PET imaging and *ex vivo* biodistribution. The SUV of [$^{11}$C]preladenant in several brain regions and peripheral organs are reported.

In **chapter 3**, the tracer kinetics in rat brain is further characterized by kinetic modeling. Several modeling methods and pharmacokinetic outcome parameters are compared to determine the most suitable model and parameter to quantify [$^{11}$C]preladenant in the rat brain. In addition, the test-retest variability in tracer uptake and the feasibility of measuring $A_{2A}R$ occupancy are investigated.

In **chapter 4**, we explore the responses of $A_{2A}R$ and $D_2R$ to the depletion of dopamine, which is the pathological hallmark of PD. In addition, the changes of $A_{2A}R$ and $D_2R$ in dopamine depleted rats in response to levodopa treatment, which is the standard treatment for PD patients, are investigated. There are two aims in this study. The first aim is to study the feasibility of [$^{11}$C]preladenant-PET to monitor the changes of $A_{2A}R$ availability at different stages of PD. If such changes can be detected, the second aim is to establish the relationship between $A_{2A}R$ and $D_2R$ availability, and their relation to motor symptoms during the course of PD. 6-

hydroxy dopamine (6-OHDA) or sham lesioned rats are used in the study. 6-OHDA lesioning in substantia nigra results in the death of >90% of the dopamine producing neurons, and the animals subsequently develop Parkinsonian-like motor symptoms. PET imaging using [$^{11}$C]preladenant and [$^{11}$C]raclopride, is performed in rats to monitor the changes of $A_{2A}R$ and $D_2R$ density in striatum after dopamine depletion and after levodopa treatment in dopamine depleted animals. Behavioral tests are performed to study cognition and the locomotor symptoms of the rats.

The previous experiments demonstrated that [$^{11}$C]preladenant is able to monitor disease- and drug-induced changes of $A_{2A}R$ availability. The tracer shows favorable pharmacokinetic profiles and high test-retest reproducibility. Using [$^{11}$C]preladenant-PET to study $A_{2A}R$ in human subjects is foreseeable. In order to bridge the gap between rodent studies and the human study, the properties of [$^{11}$C]preladenant are further studied in conscious rhesus monkeys by PET imaging (**chapter 5**). Kinetic modeling is used to quantify tracer kinetics in the monkey brain. Specific binding of the tracer to $A_{2A}R$ is studied by pretreatment of the $A_{2A}R$ subtype selective antagonists KW-6002 and unlabeled preladenant. The feasibility of [$^{11}$C]preladenant to study $A_{2A}R$ occupancy in monkey brain is assessed by pretreatment of various doses of a non-selective adenosine antagonist caffeine.

The last gap to be bridged before using [$^{11}$C]preladenant in human subjects is the dosimetry estimation. Radiation dosimetry measurement is required to determine the dose limits of a new tracer before a clinical trial can begin. Radiation dosimetry measured in rodents could be easily translated to humans. In **chapter 6**, PET imaging and *ex vivo* biodistribution in rats are applied to measure tracer concentration in tissues. The data is then used to obtain radiation dosimetry estimates in rats and in humans, and to determine the dose limit of [$^{11}$C]preladenant. Furthermore, data obtained from PET imaging is compared with data obtained from *ex vivo* biodistribution, using *ex vivo* biodistribution as the gold standard. The result of the comparison determines the usefulness of small-animal PET imaging for the estimation of radiation dosimetry.

**Chapter 7** summarizes the findings of the studies and **chapter 8** is a description of future perspectives and a conclusion.